JACS
JOURNAL OF THE AMERICAN CHEMICAL SOCIETY
Article
pubs.acs.org/JACS

Origins of Stereoselectivity in Intramolecular Aldol Reactions Catalyzed by Cinchona Amines

Yu-hong Lam and K. N. Houk*

Department of Chemistry and Biochemistry, University of California, Los Angeles, California 90095-1569, United States

Supporting Information

ABSTRACT: The intramolecular aldol condensation of 4-substituted heptane-2,6-diones leads to chiral cyclohexenones. The origins of the enantioselectivities of this reaction, disclosed by List et al. using a cinchona alkaloid-derived primary amine (cinchona amine) organocatalyst, have been determined with dispersion-corrected density functional theory (DFT). The stereocontrol hinges on the chair preference of the substrate−enamine intermediate and the conformational preferences of a hydrogen-bonded nine-membered aldol transition state containing eight heavy atoms. The conformations of the hydrogen-bonded ring in the various stereoisomeric transition structures have been analyzed in detail and shown to closely resemble the conformers of cyclooctane. A model of stereoselectivity is proposed for the cinchona amine catalysis of this reaction. The inclusion of Grimme's dispersion corrections in the DFT calculations (B3LYP-D3(BJ)) substantially improves the agreement of the computed energetics and experiment, attesting to the importance of dispersion effects in stereoselectivity.

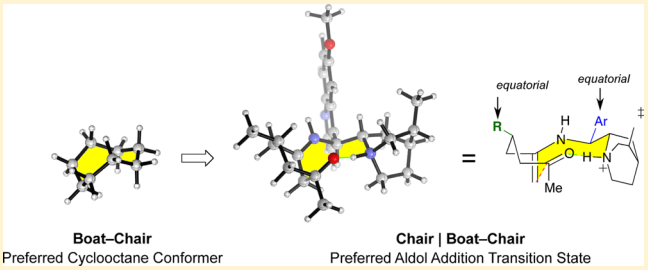

INTRODUCTION

In 2008, List reported the first highly enantioselective organocatalytic route to 5-substituted cyclohexenones (Scheme 1).[1] The quinine-derived primary amine **I**,[2] plus acetic acid as a cocatalyst, catalyzes the conversion of achiral 4-substituted heptane-2,6-diones (**1**−**3**) to chiral cyclohexenones (**7**−**9**) with high enantioselectivities via a desymmetrizing intramolecular aldol condensation. Previous methods using proline[3,4] or a catalytic antibody[5] are considerably less enantioselective. The aldol condensations organocatalyzed by **I** have been employed in the preparations of synthetic fragrance materials and other valuable chiral cyclohexenone building blocks[6] with high optical purities.[1] Highly enantioselective intermolecular aldol reactions catalyzed by cinchona alkaloid primary amines (cinchona amines) have also been reported by other groups.[7] The origin of the stereocontrol is unknown. List suggested[1] that the protonated quinine might act as a Brønsted acid for the activation of the electrophilic carbonyl group as well as for its orientation at the transition state.

Scheme 1. Selected Examples of List's Desymmetrizing Intramolecular Aldol Condensation Reactions of 4-Substituted Heptane-2,6-diones Catalyzed by I

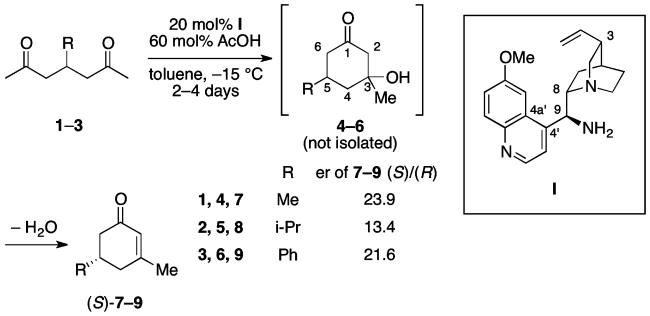

Our group previously studied the origin of asymmetric induction in proline-catalyzed intramolecular aldol reactions of **1**,[8] the Hajos−Parrish−Eder−Sauer−Wiechert reaction,[4,9] and, in collaboration with List's group, the stereoselectivities of proline-catalyzed intermolecular aldol reactions.[10−13] That work validated the strategy of dual activation of carbonyl groups by enamine formation and hydrogen bonding. This concept has extensively guided the mechanistic understanding and catalyst design in organocatalysis.[14] As shown in Scheme 2, proline serves as a bifunctional catalyst that activates the donor carbonyl component by enamine formation while forming a hydrogen bond between the carboxylic acid functionality and the electrophilic carbonyl group. The stereoselectivity-determining, C−C bond-forming aldol addition transition state is best described as a nine-membered hydrogen-bonded ring comprising the proline enamine and the acceptor carbonyl. The reacting atoms are arranged in a Zimmerman−Traxler-like fashion, and C−C bond formation is concerted with proton transfer from the carboxylic acid moiety of proline to the forming alkoxide. As shown by the Newman projections, this so-called Houk−List model features fully staggered arrangements of substituents about the forming C−C bond. The donor

Received: December 23, 2014
Published: January 28, 2015

DOI: 10.1021/ja513096x
J. Am. Chem. Soc. 2015, 137, 2116−2127

Scheme 2. (A) Partial Zimmerman−Traxler Transition State for Proline-Catalyzed Aldol Addition and (B) Seebach's Topological Rule for C−C Bond Formation between Prochirality Centers

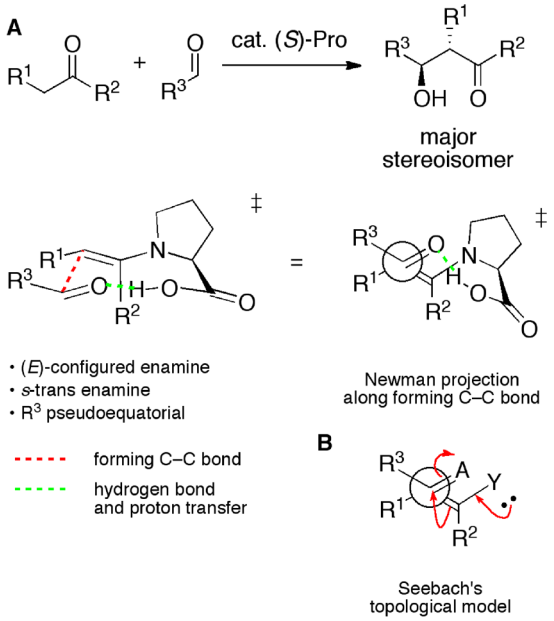

C=C and acceptor C=O bonds are synclinal, consistent with Seebach's topological rule for C−C bond formation between prochirality centers.[15]

Like proline, cinchona alkaloid derivatives have emerged as a privileged class of organocatalysts that have been employed in an ever broadening range of transformations.[16−18] Cinchona alkaloid primary amines such as **I** are especially useful for the activation of sterically encumbered carbonyl groups, with which proline is less effective.[17] However, the high levels of stereoselectivity in most of these reactions are nontrivial to rationalize. Consequently, there is a scarcity of stereochemical models proposed for the numerous transformations reported to date. Compared with proline, the cinchona alkaloid scaffold supports a richer array of functional groups and possesses higher conformational flexibility. As a result, the essential stereocontrolling factors are not conspicuous from the structure of the reactants and the organocatalysts. Considerable advances have been made recently in uncovering the reaction mechanisms and origins of stereocontrol by cinchona alkaloid-derived organocatalysts with different catalytic principles, including iminium activation,[19−22] hydrogen-bonding interactions[23−26] (including weak C−H···O interactions[27,28]), and phase-transfer catalysis.[29−33] However, in the realm of enamine-activated transformations, the mechanism by which **I** exerts stereochemical control has seldom been investigated. We recently studied the origins of asymmetric induction in the α-fluorination of cyclic ketones catalyzed by a cinchona amine, first reported by MacMillan.[34] The facial selectivity of the enamine was proposed to arise from the chair preference of the seven-membered cyclic fluorine transfer transition state. The aldol reaction is indispensable in stereoselective C−C bond formation.[35] Further, the conformational properties of cinchona alkaloids and their derivatives have been extensively investigated, starting from the pioneering work by Wynberg.[36−38] We now present quantum-chemical computations that identify the source of asymmetric induction in the desymmetrizing aldol condensations catalyzed by **I**. We also propose a stereoselectivity model to show how the conformational preferences of this ring can account for the sense and level of enantiocontrol in cyclohexenone formation.

COMPUTATIONAL METHODS

All of the quantum-chemical computations were performed using Gaussian 09.[39] The geometries were fully optimized at the B3LYP[40]/6-31G(d) level of theory in conjunction with the IEF-PCM implicit solvation model[41] to account for the solvation effects of toluene, the solvent used experimentally. All of the optimized geometries were verified by frequency computations as minima (zero imaginary frequencies) or transition structures (a single imaginary frequency). Single-point energies of the optimized geometries were then evaluated using the dispersion-corrected density functional method B3LYP-D3[42] (with a Becke−Johnson (BJ) damping function[43,44]) and the polarized, triple-ζ valence quality def2-TZVPP basis set of Weigend and Ahlrichs[45] within the IEF-PCM model (toluene). The thermal corrections evaluated from the unscaled vibrational frequencies at the B3LYP/6-31G(d) level on the optimized geometries were then added to the B3LYP-D3(BJ)/def2-TZVPP electronic energies to obtain the free energies. The free energy corrections were calculated using Truhlar's quasiharmonic approximation.[46] This uses the usual harmonic oscillator approximation in the calculations of the vibrational partition functions, except that all of the real vibrational frequencies that are lower than 100 cm^{-1} are set to 100 cm^{-1} as a way to correct for the spurious overestimation of vibrational entropies introduced by treating low-frequency vibrational modes as harmonic oscillators. Single-point energies were also calculated within the IEF-PCM model at the B3LYP/def2-TZVPP, M06-2X[47]/def2-TZVPP, and M06-2X-D3(zero damping)[44]/def2-TZVPP levels on B3LYP/6-31G(d) geometries to compare the stereoselectivities computed by various dispersion-inclusive and -uncorrected functionals.

The B3LYP/6-31G(d) method has a very strong track record in modeling a wide variety of organocatalytic reactions,[48] including the proline-catalyzed aldol reaction.[4,8−11] More recently, the shortcomings of B3LYP and other early density functionals in accounting for London dispersion have been noted.[49] Nevertheless, for 19 covalent-bond-forming stereoselective organic reactions, including organocatalytic systems, Simón and Goodman[50] compared the stereoselectivities computed using various density functionals and found that for transition-structure geometry optimizations, B3LYP is generally only slightly less accurate than the newer, dispersion-inclusive functionals, which are somewhat more computationally demanding.[51] To calculate the energies of stereoselectivity-determining transition structures, they recommended evaluating single-point energies using a dispersion-inclusive functional (M05-2X) on B3LYP-optimized geometries as an efficient compromise between accuracy and computational cost. Recently, Krenske and Houk[52] re-evaluated the theoretical stereoselectivities for seven organic and organometallic reactions using B3LYP-D3 and M06-2X single-point energies of the stereoselectivity-determining transition structures optimized at the B3LYP/6-31G(d) level. Satisfactory agreements with the experimental stereoselectivities were obtained. Recent work from our group[53] and others[54] also showed that B3LYP geometry optimizations coupled with single-point energy evaluations using a dispersion-inclusive density functional give good agreement with experimental stereoselectivities for a variety of organic reactions. Here we used the D3(BJ)-corrected B3LYP and M06-2X (with and without D3(zero) corrections) functionals with the def2-TZVPP basis set to derive dispersion-inclusive single-point energies on B3LYP/6-31G(d) geometries. B3LYP-D3(BJ)/def2-TZVPP−IEF-PCM//B3LYP/6-31G(d)−IEF-PCM results are presented in the main text, while results involving M06-2X and M06-2X-D3(zero) single-point energies are discussed in the Supporting Information (SI). The use of a large basis set has been recommended in order to minimize basis set superposition errors and to achieve high accuracies in the computations of dispersion energies.[55]

To identify the lowest-energy conformers of the enamine reactants and the reactive conformations for intramolecular aldol addition,

DOI: 10.1021/ja513096x
J. Am. Chem. Soc. 2015, 137, 2116−2127

Monte Carlo conformational searches were performed on the enamines derived from diketones **1** and **10** and the model catalysts **II** and **III** (Chart 1) protonated at the quinuclidine nitrogen using

Chart 1. Structures of Model Reactant 10 and Model Catalysts II and III

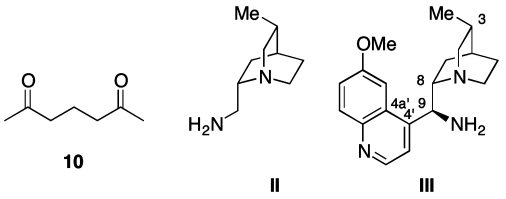

Macromodel 9.9[56] with the OPLS-2005 force field.[57] Structures in which the distance between the bond-forming carbons is shorter than 4.0 Å were used in transition-structure searches. Some of the DFT-optimized transition structures obtained in this way were manually modified to generate additional input geometries for the optimization of stereoisomeric or differently substituted transition structures.

RESULTS AND DISCUSSION

As summarized in Scheme 1, the optimized conditions reported by List[1] for the intramolecular aldol condensation reactions of acyclic 2,6-diketones such as **1**–**3** employ 20 mol % organocatalyst **I**, 60 mol % acetic acid as a cocatalyst, and toluene as the solvent. Among the screened cocatalysts that were used in 3-fold excess and brought about full conversion within 36–48 h, similar enantioselectivities (20.1:1 to 17.8:1) were reported for acetic, propionic, isobutyric, and benzoic acids, despite the different shapes and sizes of these cocatalysts. Thus, among the most effective cocatalysts, the counterion has only a minor influence on the enantiocontrol (the $\Delta\Delta G^{\ddagger}$ values vary by <0.23 kcal/mol as the counterion is changed) and was omitted in our computations of the stereoisomeric transition states here.[58]

Use of the quinidine-derived catalyst **I′** (Chart 2) in lieu of quinine-derived **I** has been reported to invert the absolute

Chart 2. Structures of Organocatalysts I and I′

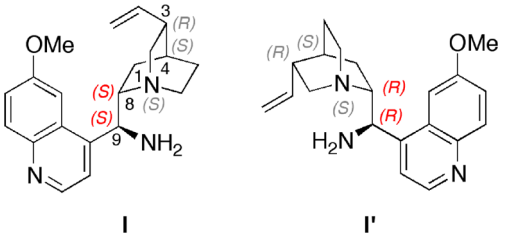

configuration of the cyclohexenones, and the levels of enantioselectivity remain similar.[1] **I** and **I′** possess opposite configurations only at C8 and C9 (highlighted in red). These centers control the sense of asymmetric induction. The configurations of the other three chirality centers in **I** and **I′** (N1, C3, and C4) are unimportant.

Baiker has demonstrated by NMR titration experiments that in the presence of 2 equiv of acetic acid in ethanol, cinchonidine is protonated at the quinuclidine nitrogen to about 95% and the quinoline nitrogen is not protonated.[59] This is in line with expectations from the pK values of cinchonine (pK_1 = 5.80, pK_2 = 10.3).[60] Thus, in our work, the quinuclidine nitrogen was always protonated.

The enamine activation of carbonyl groups for the aldol reaction is well-established.[9,61] The catalytic cycle for the intramolecular aldol cyclizations of **1**–**3** catalyzed by **I** is shown in Scheme 3. Diketones **1**–**3** react, through either of the two

Scheme 3. Catalytic Cycle for Aldol Cyclizations of 1–3 Catalyzed by I

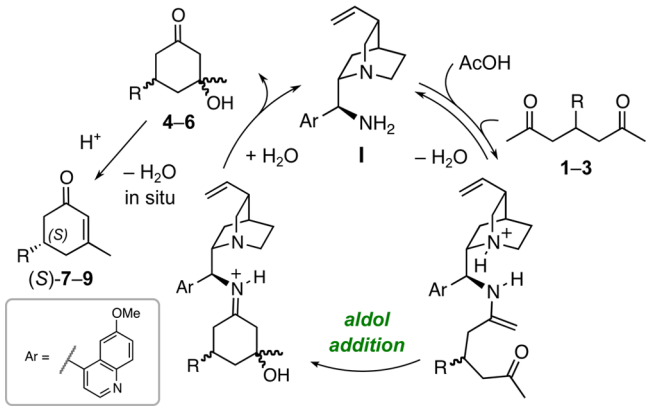

enantiotopic carbonyl groups, with the primary amine of the protonated organocatalyst to reversibly generate an enamine intermediate. Intramolecular aldol addition followed by hydrolysis of the iminium ion furnishes the cyclized products **4**–**6**, which undergo rapid dehydration in situ to yield the enantioenriched cyclohexenones **7**–**9**. Only traces of **4**–**6** were detected under the reaction conditions,[1] and the stereoselectivities for the formation of these products have not been reported.

For this study, we assumed the aldol C–C bond formation to be the stereocontrolling step. The rates of formation of the enamines from attack of the primary amine of **III** on one or the other carbonyl group of **1** were also modeled. The details are given in the SI,[62] but the results were found to predict the wrong sense of enantioselectivity of cyclohexenone formation, ruling out the possibility that stereocontrol occurs during enamine formation.

Key similarities in structure and relative stability trends were found for the stereoisomeric aldol cyclization transition states **TS-10** involving heptane-2,6-dione (**10**) catalyzed by model catalyst **II** protonated at the quinuclidine nitrogen (Chart 1) and those for diketones **1**–**3** catalyzed by **I** (**TS-1**, **TS-2**, and **TS-3**). Thus, we examine the set of transition structures **TS-10** first, followed by the results involving **1**–**3** and catalyst **I**.

1. Stereoisomeric Transition Structures for Aldol Cyclizations of 10 Catalyzed by II. Figures 1 and 2 illustrate the transition structures in which the incipient six-membered ring adopts a chair conformation (**TS-10a**–**d**) or a boat conformation (**TS-10e**–**h**), respectively. **TS-10a**, **TS-10d**, **TS-10e**, and **TS-10h** lead to the *S* enantiomer of aldol **11**, while **TS-10b**, **TS-10c**, **TS-10f**, and **TS-10g** give rise to (*R*)-**11**.

The aldol C–C bond-forming step is accompanied by proton transfer from the quinuclidinium moiety and has an activation free energy ($\Delta G^{\ddagger}$) of 12.9 kcal/mol (**TS-10a**). The lowest-energy transition structures that give (*S*)-**11** and (*R*)-**11** are **TS-10a** and **TS-10c**, respectively, and the energy difference between them is 2.6 kcal/mol in favor of **TS-10a**. The forming six-membered ring is found to preferentially adopt a chair conformation. The boat transition structures **TS-10e**–**h** (Figure 2) are all at least 4.9 kcal/mol less stable than **TS-**

DOI: 10.1021/ja513096x
J. Am. Chem. Soc. 2015, 137, 2116–2127

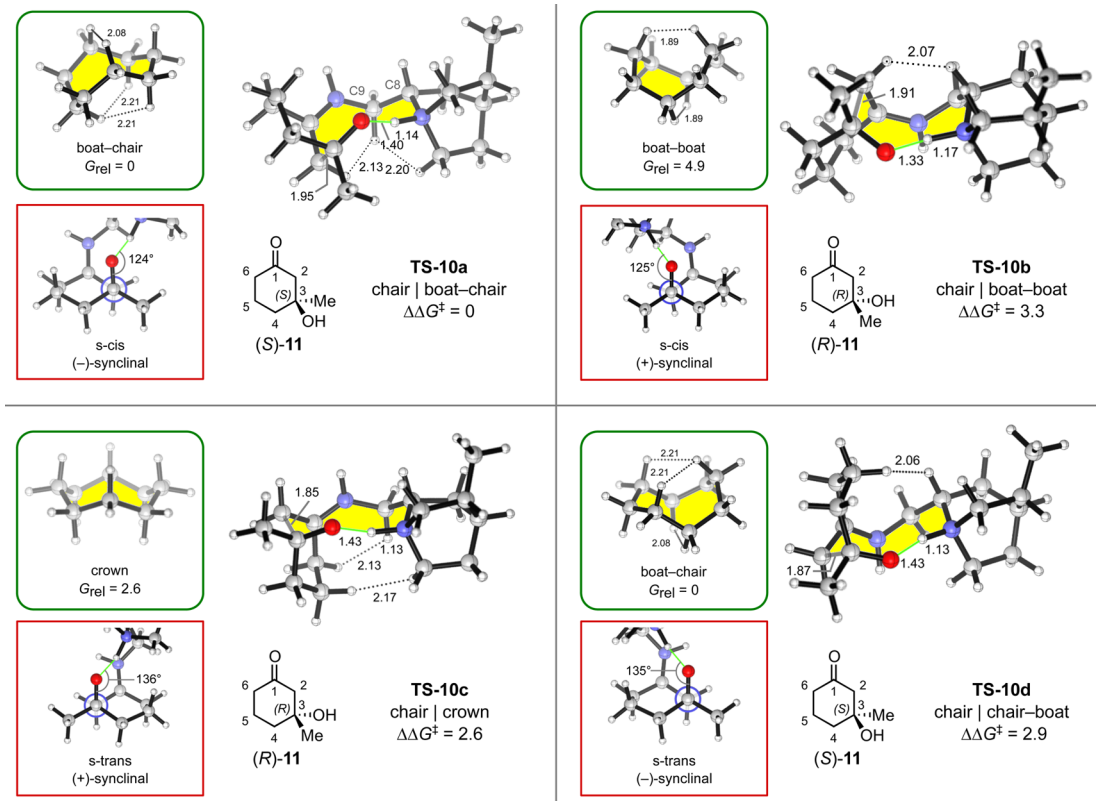

Figure 1. Chair transition structures (**TS-10a–d**) for the intramolecular aldol reaction of heptane-2,6-dione (**10**) catalyzed by model catalyst **II** (B3LYP-D3(BJ)/def2-TZVPP–IEF-PCM(toluene)//B3LYP/6-31G(d)–IEF-PCM(toluene)). Each transition structure is described by two conformational designators that refer to the forming six-membered ring and the medium ring. The relative free energies of activation compared with **TS-10a** ($\Delta\Delta G^{\ddagger}$) are reported in kcal/mol. In the illustrations, the close H–H contacts (<2.20 Å) are annotated and the hydrogen-bonded nine-membered rings are color-filled. The resulting enantiomer of **11** for each transition structure is also shown. Green insets: Analogous cyclooctane conformers and relative free energies (CCSD(T)/6-311++G**) reported by Wiberg (ref 64). Red insets: Newman projections along the forming C–C bond. The rotameric states of the enamine N–C bond (s-cis or s-trans) and the C=C···C=O partial bond ((+)- or (–)-synclinal) are labeled.

10a. **TS-10a** is lower in energy than all of the other chair transition structures by at least 2.6 kcal/mol, while **TS-10b**, **TS-10c**, and **TS-10d** have stabilities within 0.7 kcal/mol of one another. Within the boat family of transition structures (**TS-10e–h**; Figure 2), **TS-10f** is the most destabilized ($\Delta\Delta G^{\ddagger}$ = 7.1 kcal/mol relative to **TS-10a**), whereas the other transition structures **TS-10e**, **TS-10g**, and **TS-10h** have comparable stabilities within 0.5 kcal/mol of one another.

All of the transition structures in Figures 1 and 2 contain a hydrogen-bonded nine-membered ring comprising the electrophilic carbonyl group, the enamine, and its parent organocatalyst. An essential feature shared by the transition structures for the aldol additions catalyzed by both proline and the cinchona alkaloid primary amines is proton transfer from the carboxylic acid of proline or the quinuclidinium moiety of the N-protonated cinchona amine. Regardless of the rotameric state of the enamine, an effective proton-transfer geometry is preserved with respect to both the proton donated (N–H–O bond angles of 163–174°) and the carbonyl oxygen (H–O–C bond angles of 124–136°). Maximal staggering about the forming C–C bond is also maintained.[63] Thus, the optimized structures of **TS-10a–h** are all in accord with Seebach's topological rule.[15]

To further understand the geometries and relative energies of the transition structures, it is instructive to examine the geometries of the medium rings in detail. *A striking feature of* ***TS-10a–h*** *is that the heavy (i.e., non-hydrogen) atoms in the medium rings are arranged analogously to the carbon atoms in the conformational minima of cyclooctane.*[64−69] In Figures 1 and 2, the transition structures' medium rings are color-filled and compared to the corresponding cyclooctane conformers, which are shown in the green insets. The medium rings of **TS-10a** and **TS-10e** adopt a boat–chair conformation in which the boat moiety is composed of the enamine and the C=O bond. A boat–boat conformation is found in **TS-10b** and **TS-10f**. **TS-10c** and **TS-10g** contain a crown conformation, while **TS-10d** and **TS-10h** display a chair–boat conformation with the enamine and C=O bond forming the chair moiety.

The conformational analysis of cyclooctane has been the subject of many experimental and computational investigations.[64−69] Cyclooctane is known to exist at room temperature in predominantly two families of conformations, the boat–chair and the crown, in a ratio of 94:6.[69] Quantum-chemical computations have also established the boat–chair conformation as the global minimum, although different numbers of conformational minima have been reported depending on the computational method.[64,65] At the CCSD(T)/6-311++G** level of theory, the crown and boat–boat conformations are 2.6 and 4.9 kcal/mol less stable than the boat–chair conformation, respectively.[64,70] These values are given in the green insets in Figure 1.

The medium ring in the most favored aldol addition transition structure, **TS-10a**, adopts the conformation of the boat–chair cyclooctane that is the most stable. This is

DOI: 10.1021/ja513096x
J. Am. Chem. Soc. 2015, 137, 2116–2127

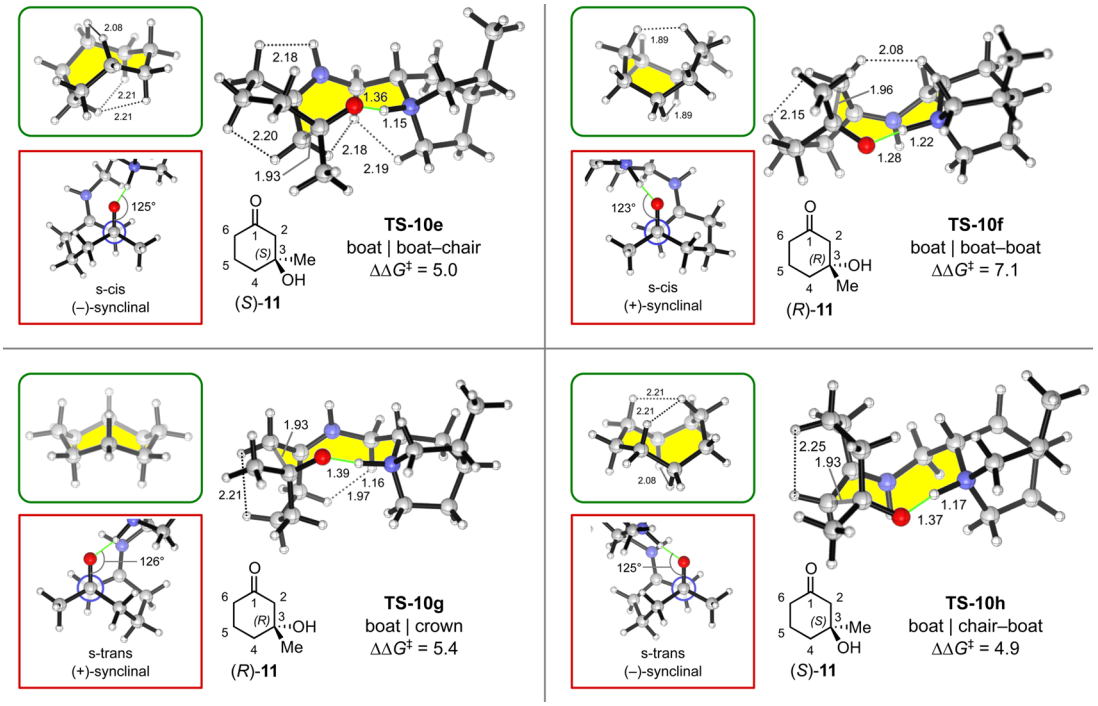

Figure 2. Boat transition structures (**TS-10e–h**) for the intramolecular aldol reaction of heptane-2,6-dione (**10**) catalyzed by model catalyst **II** (B3LYP-D3(BJ)/def2-TZVPP–IEF-PCM(toluene)//B3LYP/6-31G(d)–IEF-PCM(toluene)). Each transition structure is described by two conformational designators that refer to the forming six-membered ring and the medium ring. The relative free energies of activation compared with **TS-10a** (see Figure 1) ($\Delta\Delta G^{\ddagger}$) are reported in kcal/mol. In the illustrations, the close H–H contacts (<2.20 Å) are annotated and the hydrogen-bonded nine-membered rings are color-filled. The resulting enantiomer of **11** for each transition structure is also shown. Green insets: Analogous cyclooctane conformers reported by Wiberg (ref 64). Red insets: Newman projections along the forming C–C bond. The rotameric states of the enamine N–C bond (s-cis or s-trans) and the C=C···C=O partial bond ((+)- or (–)-synclinal) are labeled.

reminiscent of the Zimmerman–Traxler model for metal enolate aldol additions,[71] in which a six-membered cyclic transition state prefers a chair conformation.

The relative energies of the aldol addition transition structures are the result of intricate trade-offs between transannular interactions, eclipsing strain, and other steric interactions within the medium rings in different conformations. Some of these interactions can be understood by comparison to the corresponding conformers of cyclooctane. For example, in **TS-10a** and **TS-10e,** a close steric contact that can be compared to the 1,4-diaxial interaction in the boat–chair cyclooctane is present between the *Z* hydrogen of the s-cis enamine (H2) and a hydrogen on C9. **TS-10b** and **TS-10f** are destabilized by a steric clash between H2 and a hydrogen on C8, analogous to the 1,5-transannular (flagpole) interaction that characterizes the boat–boat cyclooctane. Additional steric interactions between the cyclizing moiety and the catalyst are present. For instance, **TS-10d** is destabilized by a steric clash between the C5 methylene group and the axial C8 hydrogen on the chair–boat medium ring. The boat transition structures, **TS-10e–h**, are at least 4.9 kcal/mol less stable than the lowest-energy structure **TS-10a**. Flagpole interactions within the forming six-membered ring dominate the relative stabilities of **TS-10e**, **TS-10g**, and **TS-10h**. **TS-10f** is the most destabilized ($\Delta\Delta G^{\ddagger}$ = 7.1 kcal/mol) because of flagpole interactions in both the six- and nine-membered rings.

2. Stereoselectivities of Experimental Systems. The origin of the stereocontrol in the experimentally reported intramolecular aldol condensations of **1** (Scheme 1) was then investigated.

2.1. Conformations of the Organocatalyst and Enamines. The conformations of cinchona alkaloids and their derivatives have been extensively analyzed spectroscopically and computationally.[36−38] Four principal conformations arising from rotation about the C8–C9 and C9–C4′ single bonds have been identified, as shown in Scheme 4 for the cinchona alkaloid primary amine **I**. The terms *open* and *closed* refer to the rotameric state about the C8–C9 bond.[36] In an *open* conformation, the quinuclidine nitrogen lone pair points away from the quinoline ring and there is an anti arrangement about the C8–C9 bond. In a *closed* conformation, the lone pair points toward the quinoline with a gauche arrangement about the C8–C9 bond. *Syn* and *anti* describe the orientation of the quinoline ring by referring to the torsional arrangement of the C9–C4′ bond with regard to the heteroatom bonded to C9 (nitrogen in **I**) and the quinoline's ring junction carbon C4a′. For catalyst **I**, the quantum-chemical computations of Melchiorre found that the *open* conformers are more stable than the *closed* conformers by at least 5.4 kcal/mol and that the *anti-open* and *syn-open* conformers have comparable energies (Scheme 4).[20]

We used catalyst **III** as a model of the experimentally used organocatalyst **I**. **III** and **I** differ only in the replacement of the vinyl group by a methyl group (Scheme 1). This replacement greatly reduces the number of different conformers that require investigation.[72] The most stable conformers of enamines **12a** and **12b** derived from condensation of the primary amine of the N-protonated catalyst **III** and either enantiotopic carbonyl group of **1** are predicted to have comparable stabilities (Figure 3). *Closed*-type conformers of **12a** and **12b** could not be located in the conformational searches. These geometries are higher in

DOI: 10.1021/ja513096x
J. Am. Chem. Soc. 2015, 137, 2116–2127

Scheme 4. Conformers of Catalyst I[a]

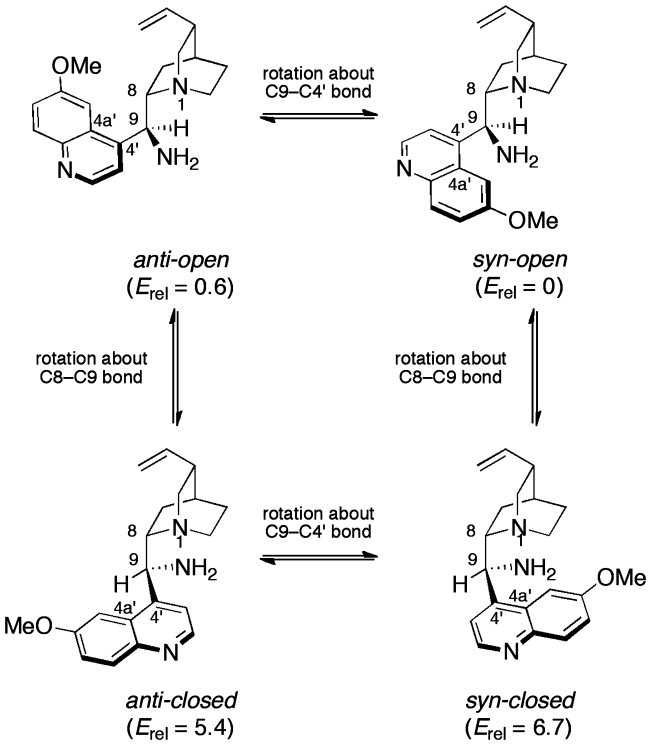

[a]Energies (BP86-D/TZP, in kcal/mol) were taken from ref 20.

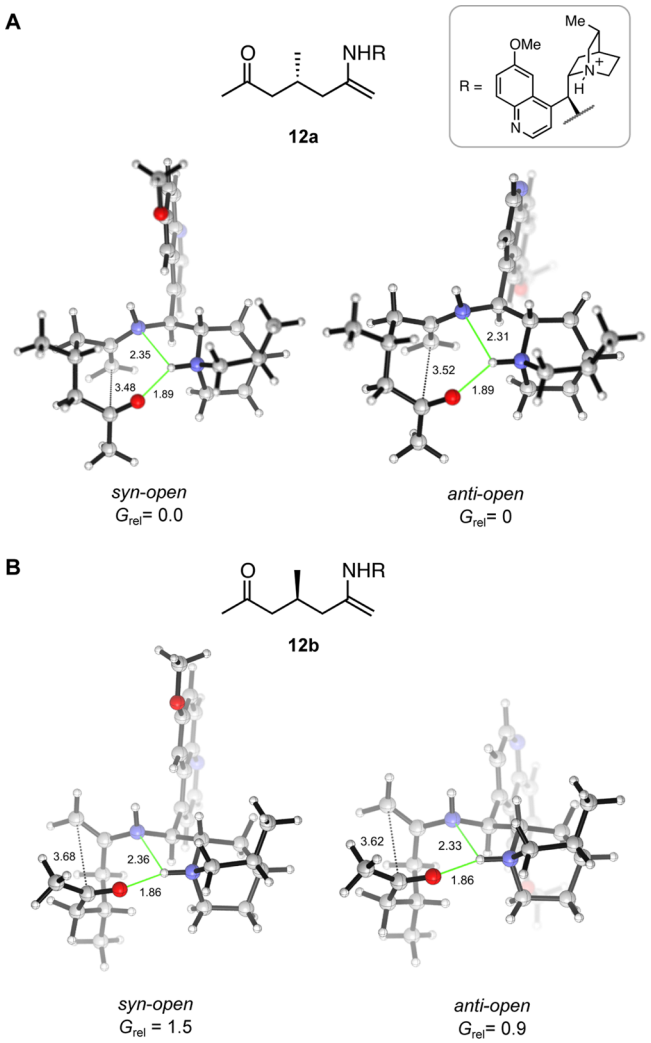

Figure 3. Most stable conformers of protonated enamines (A) **12a** and (B) **12b** formed from **1** and model catalyst **III** (B3LYP-D3(BJ)/def2-TZVPP–IEF-PCM(toluene)//B3LYP/6-31G(d)–IEF-PCM-(toluene)). The free energies relative to *anti-open*-**12a** (G_{rel}) are reported in kcal/mol.

energy because the quinoline ring is synclinal to the ring C–C and C–N^+ bonds, and the hydrogen bond from the quinuclidinium ion to the ketone oxygen cannot be maintained. The overwhelming prevalence of *open* over *closed* conformers of the protonated enamines found here is consistent with the effect of protonation on the conformation of cinchonidine reported by Mueller and Zaera,[38] who observed that the conformational space of the cinchonidinium ion is restricted to the *open* states only.

2.2. Stereoisomeric Transition Structures for Aldol Cyclization of 1. For each of the four stereoisomers of aldol adduct **4**, four transition-state conformers that combine different conformations of the forming six-membered ring and the hydrogen-bonded nine-membered ring were located, resulting in a total of 16 transition structures (**TS-1a–p**). The lowest-energy transition structures that lead to the four stereoisomeric aldols (**TS-1a–d**) are illustrated in Figure 4. For **TS-1a–d**, transition structures differing only in the orientation of the quinoline ring, that is, the *syn* versus *anti* conformation (**TS-1a′–d′**) were also located and found to differ by less than 0.7 kcal/mol. Details concerning all of these transition structures are discussed in the SI. For each stereoisomer of **4**, only one transition structure needs to be considered since the other three conformers are significantly higher in energy (Table S1 in the SI). The ring conformations found for the truncated system (diketone **10** and model catalyst **II**) are all retained in **TS-1a–d**, while the cinchona amine moiety adopts an *open* conformation. The medium rings in the lowest-energy transition structures have either boat–chair or crown conformations, and the *S*-configured quinoline ring of the catalyst is equatorial.

Experimentally, the intramolecular aldol condensation of **1** catalyzed by **I** produces (*S*)-**7** as the major product with an enantiomeric ratio of 23.9 (Scheme 1).[1] The diastereoselectivity of the formation of **4** has not been reported; only traces of **4** were detected under the reaction conditions as a result of in situ dehydration. Our computations predict that the aldol addition step through **TS-1a** is the most facile among the stereoisomeric pathways, with a free energy of activation ($\Delta G^{\ddagger}$) of 12.6 kcal/mol. **TS-1a** and **TS-1d** lead to (3*S*,5*S*)-**4** and (3*R*,5*S*)-**4**, respectively. Both of them afford the *S* enantiomer of cyclohexenone **7** after dehydration. **TS-1b** and **TS-1c**, which give rise to (3*R*,5*R*)-**4** and (3*S*,5*R*)-**4**, respectively, are responsible for the formation of (*R*)-**7**. The lowest-energy transition structures giving rise to (*S*)-**7** and (*R*)-**7** after dehydration are **TS-1a** and **TS-1b**, respectively. **TS-1a** is preferred over **TS-1b** by 1.6 kcal/mol, in very good agreement with the experimental value (1.6 kcal/mol).

The energies and geometries of the aldol TSs of **1** are readily understood by comparison to **TS-10a–h** shown in Figures 1 and 2. The chair | boat–chair conformation, as found in **TS-10a**, is the most favorable. For the aldol addition of **1**, **TS-1a** is lowest in energy because it retains this chair | boat–chair arrangement while placing both the C5 methyl and C9

DOI: 10.1021/ja513096x
J. Am. Chem. Soc. 2015, 137, 2116–2127

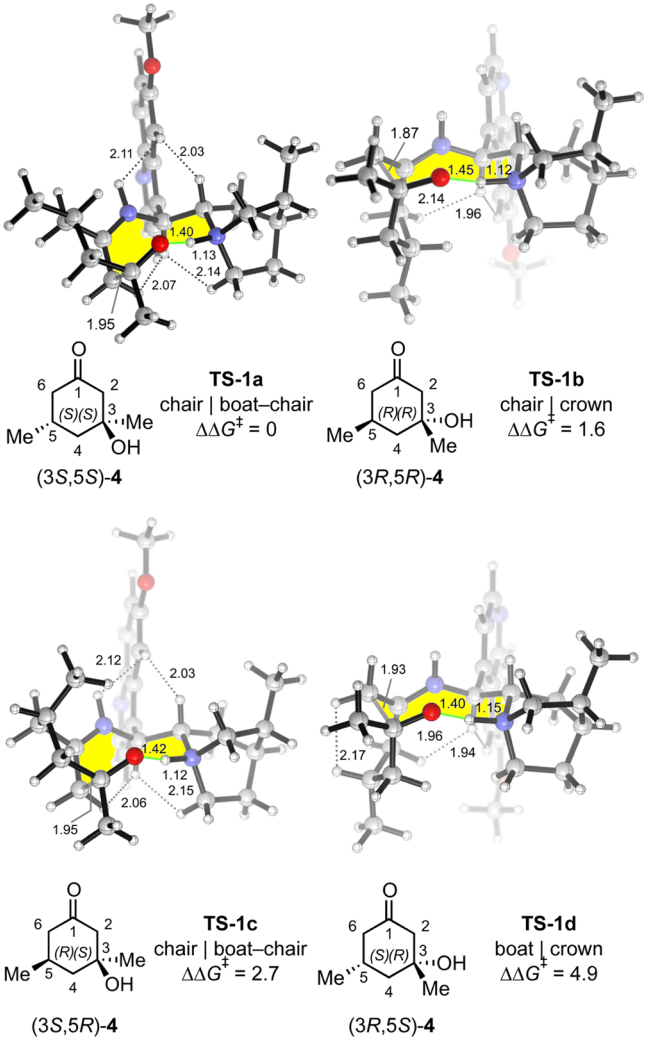

Figure 4. Lowest-energy aldol transition structures (**TS-1a–d**) of diketone **1** involving model catalyst **III** (B3LYP-D3(BJ)/def2-TZVPP–IEF-PCM(toluene)//B3LYP/6-31G(d)–IEF-PCM-(toluene)) for the formation of the four stereoisomers of **4**. The two conformational designators for each transition structure refer to the forming six-membered ring and the medium ring. The relative free energies of activation compared with **TS-1a** ($\Delta\Delta G^{\ddagger}$) are reported in kcal/mol. In the illustrations, the close H–H contacts (<2.20 Å) are annotated and the hydrogen-bonded nine-membered rings are color-filled.

quinoline groups at equatorial sites. Indeed, the free energy of activation of **TS-1a** is nearly equal to that involving unsubstituted **TS-10a**.

The alternative aldol stereoisomer that affords (*S*)-**7**, (3*R*,5*S*)-**4**, has a substantially higher barrier of formation (**TS-1d**; $\Delta\Delta G^{\ddagger}$ = 4.9 kcal/mol relative to **TS-1a**) and does not contribute to the production of **7** under the experimental conditions. **TS-1d** is based on the boat | crown geometry, which is intrinsically disfavored, as reflected by the high energy of its unsubstituted analogue **TS-10g** relative to the chair | boat–chair transition structure **TS-10a** ($\Delta\Delta G^{\ddagger}$ = 5.4 kcal/mol relative to **TS-10a**; Figure 2).

Two stereoisomers of **4**, (3*R*,5*R*) and (3*S*,5*R*), possess an *R* chirality center at C5 and give the minor cyclohexenone enantiomer (*R*)-**7** after dehydration. As shown in Figure 4, **TS-1b** and **TS-1c** are 1.6 and 2.7 kcal/mol less favored than **TS-1a**, respectively. **TS-1b** positions the C5 methyl group equatorial, but it is based on a disfavored chair | crown system (cf. the unsubstituted analogue **TS-10c**, which has $\Delta\Delta G^{\ddagger}$ = 2.6 kcal/mol relative to **TS-10a**; Figure 1). **TS-1c** retains the preferred chair | boat–chair system as found in **TS-1a**, but it suffers destabilization from the axial C5 methyl group.

2.3. Stereoselectivity-Determining Transition Structures for Aldol Cyclizations of 2 and 3. The enantioselectivities of the aldol condensations of heptane-2,6-diones substituted at C4 with different groups were also investigated. For the 4-isopropyl- and 4-phenyl-substituted diketones (**2** and **3**, respectively), the three important stereoselectivity-determining transition structures are illustrated in Figures 5 and 6,

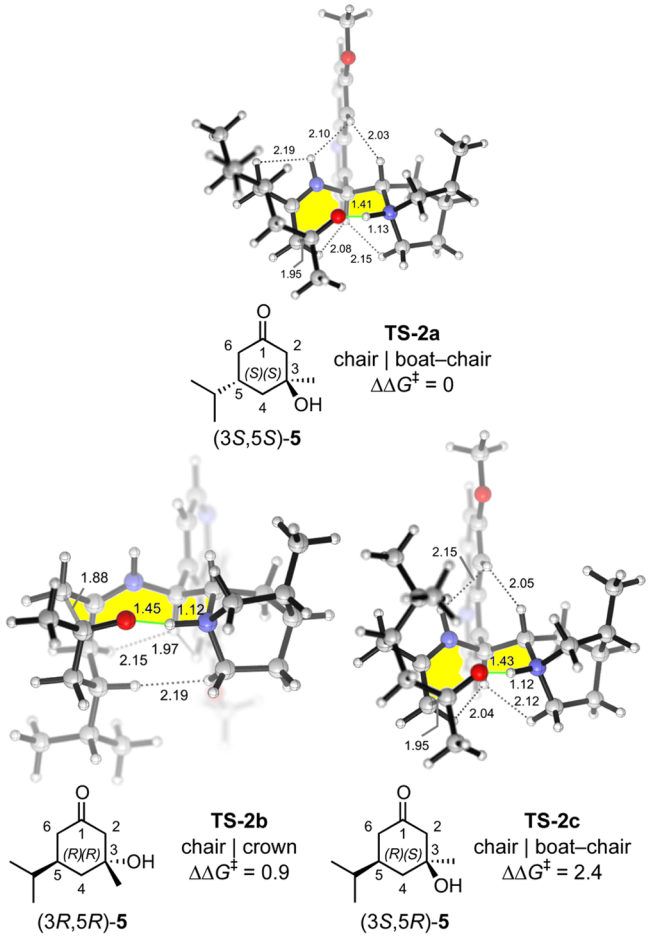

Figure 5. Lowest-energy stereoisomeric aldol addition transition structures (**TS-2a–c**) of diketone **2** involving model catalyst **III**.

respectively. Type **a** transition structures install the *S* chirality center of the cyclohexenone products **8** and **9** via the (3*S*,5*S*) aldols **5** and **6**, respectively. Transition structures of types **b** and **c** are responsible for the formation of the *R* cyclohexenones. For the aldol condensation of **2**, the chair | boat–chair transition structure **TS-2a** is 0.9 kcal/mol more stable than the chair | crown structure **TS-2b**, which is the lowest-energy transition structure that gives rise to (*R*)-**8**. This slightly underestimates the experimental enantioselectivity (1.3 kcal/mol from an *S*/*R* ratio of 13.4; Scheme 1). The chair | boat–chair transition structure **TS-2c** has a $\Delta\Delta G^{\ddagger}$ value of 2.4 kcal/mol. For **3**, the free energy difference of 1.5 kcal/mol between **TS-3a** and **TS-3b** is also in good agreement with the experimental value (1.5 kcal/mol; *S*/*R* = 21.6).

DOI: 10.1021/ja513096x
J. Am. Chem. Soc. 2015, 137, 2116–2127

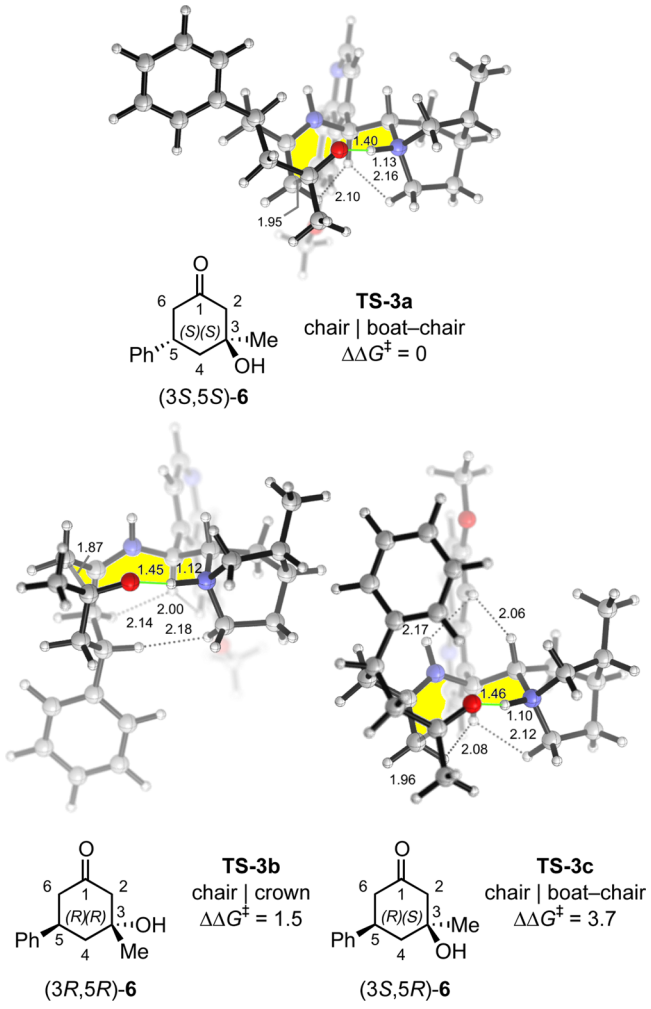

Figure 6. Lowest-energy stereoisomeric aldol addition transition structures (**TS-3a–c**) of diketone **3** involving model catalyst **III**.

2.4. Summary of the Origins of Enantiocontrol. Scheme 5 summarizes the factors responsible for the stereocontrol in the desymmetrizing aldol condensation reactions of **1–3** catalyzed by organocatalyst **III**. Only the lowest-energy transition structures are included. In all of the transition structures, the bulky quinoline ring is accommodated at an equatorial site. The enamine formation and intramolecular aldol addition steps forge chirality centers at C5 and C3 of the aldol adduct. (The configuration at C3 is, of course, inconsequential because of the ensuing dehydration step.) The configuration at these two carbons is controlled by two factors simultaneously: (1) the disposition of the diketone substituent (the R group) on the forming chair cyclohexane (axial vs equatorial) and (2) the conformation of the hydrogen-bonded medium ring (boat–chair vs crown). *The unique combination of two energetically favorable features, namely, an equatorial R group and a chair | boat–chair ring, renders* ***TS-1a/2a/3a*** *the most favored among all of the transition structures* (Scheme 5). This explains the absolute configuration of the predicted major aldol adducts (3*S*,5*S*)-**4–6** as well as the C5 stereochemistry of the experimentally observed major cyclohexenones (*S*)-**7–9**. With regard to the origin of the enantiocontrol, an equatorial R group on a forming chair cyclohexane ring may also lead to an *R* configuration at C5 in the aldol, as shown in **TS-1b/2b/3b**, but the medium ring in this case has the less favored crown conformation. This makes it clear that the conformation of the medium ring is pivotal in controlling the sense of asymmetric induction. The *R* cyclohexenone enantiomer may also arise from **TS-1c/2c/3c**, in which the medium ring has the preferred chair | boat–chair conformation but the R group is axial. To sum up, *the transition structures leading to the minor R enantiomer of the cyclohexenone are higher in energy because the conformational preference of the medium ring and the steric preference of the diketone substituent are mismatched.*

2.5. Stereoselectivity Prediction for Aldol Cyclization of ***1*** *with Organocatalyst* ***II.*** From the analysis summarized in Scheme 5, it follows that the quinoline ring of the organocatalyst is less important in determining the stereocontrol because of its equatorial disposition on the medium ring at the aldol addition transition state. Figure 7 illustrates the stereoselectivity-determining transition structures **TS-13a–d** for the aldol cyclization of diketone **1** catalyzed by **II**, which is devoid of the quinoline ring. **TS-13a–d** are remarkably similar to **TS-1a–d** (Figure 4) with respect to both geometry and relative energy. The chair | boat–chair transition structure in which the methyl group is equatorial (**TS-13a**) is lowest in energy. The chair | crown transition structure with an equatorial methyl group (**TS-13b**) is 2.1 kcal/mol higher in energy than **TS-13a**. **TS-13c** and **TS-13d** are 2.4 and 5.3 kcal/mol less stable. **TS-13a** leads to the formation of the (3*S*,5*S*) stereoisomer of aldol **4** and, after dehydration, cyclohexenone (*S*)-**7**, while **TS-13b** leads to (*R*)-**7** via (3*R*,5*R*)-**4**. Thus, our calculations predict that the truncated cinchona amine catalyst **II** should promote the intramolecular aldol condensation of **1** with high enantioselectivities even though the quinoline ring is absent.[73–75]

3. Dependence of Stereoselectivity on Dispersion.

The importance of dispersion interactions in accurate computations of organic structures by DFT has been appreciated more widely.[49,51,52,76,77] The serious underestimation or even absence of medium- and long-range dispersion forces is a main limitation of early density functional approximations, including B3LYP.[77] These errors accumulate with increasing system size and become significant for DFT modeling of typical organocatalytic reactions.[78] Early work by Clemente and Houk[4] found that B3LYP/6-31G(d) consistently overestimates the enantioselectivities of amino acid-catalyzed aldol cyclizations as a result of the overly repulsive character of this density functional for van der Waals interactions. Recently, Rzepa and co-workers[13] studied the effects of dispersion interactions on the stereoselectivities of the proline-catalyzed aldol reaction by comparing the Houk–List transition structures[11] optimized by B3LYP and B3LYP-D3. D3 corrections in general decrease the energy differences between the stereoisomeric transition states, but the impact on the predicted stereoselectivities was nearly negligible for the systems originally studied by Houk and List.[11]

We investigated the extent to which the stereoselectivities of the aldol cyclizations here depend on dispersion interactions. Table S2 in the SI compares the differences in free energies ($\Delta\Delta G^{\ddagger}$) of the stereoisomeric aldolization transition structures of **10** catalyzed by model catalyst **II** as well as those of diketones **1–3** catalyzed by **III**. B3LYP/6-31G(d)–IEF-PCM-(toluene) geometries and thermal corrections were used. The single-point energies were evaluated within the IEF-PCM model employing the dispersion-inclusive density functionals B3LYP-D3(BJ), M06-2X, and M06-2X-D3(zero) in conjunction with the large def2-TZVPP basis set. As described in more

DOI: 10.1021/ja513096x
J. Am. Chem. Soc. 2015, 137, 2116–2127

Scheme 5. Origins of the Enantiocontrol in the Desymmetrizing Aldol Condensation of 1−3 Catalyzed by III

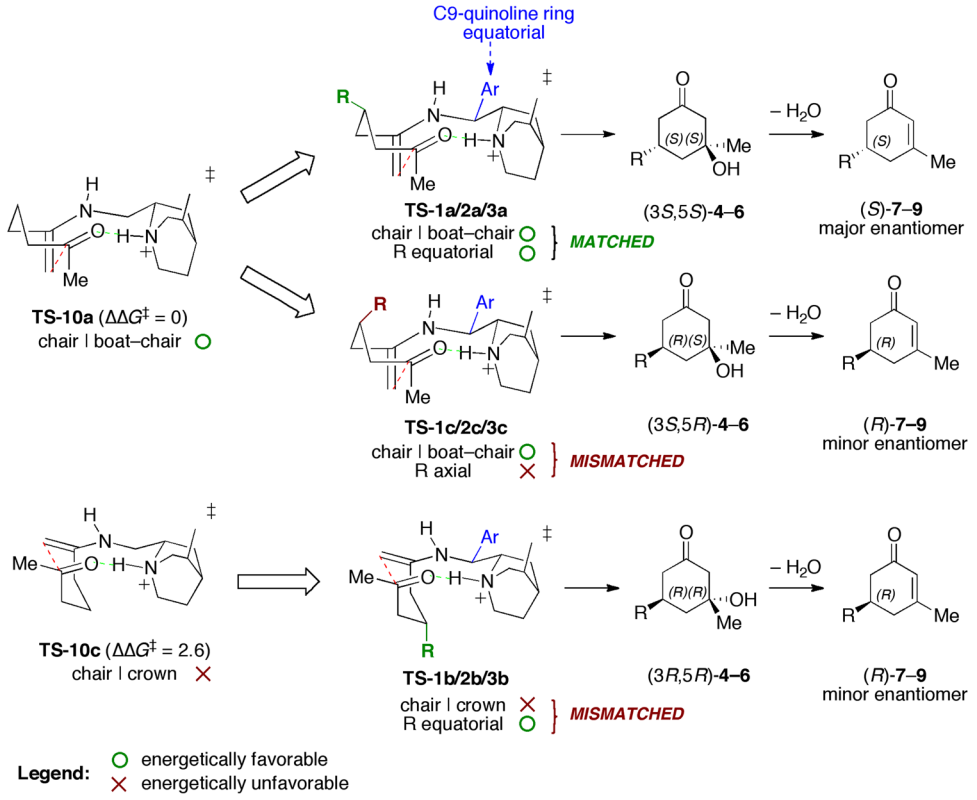

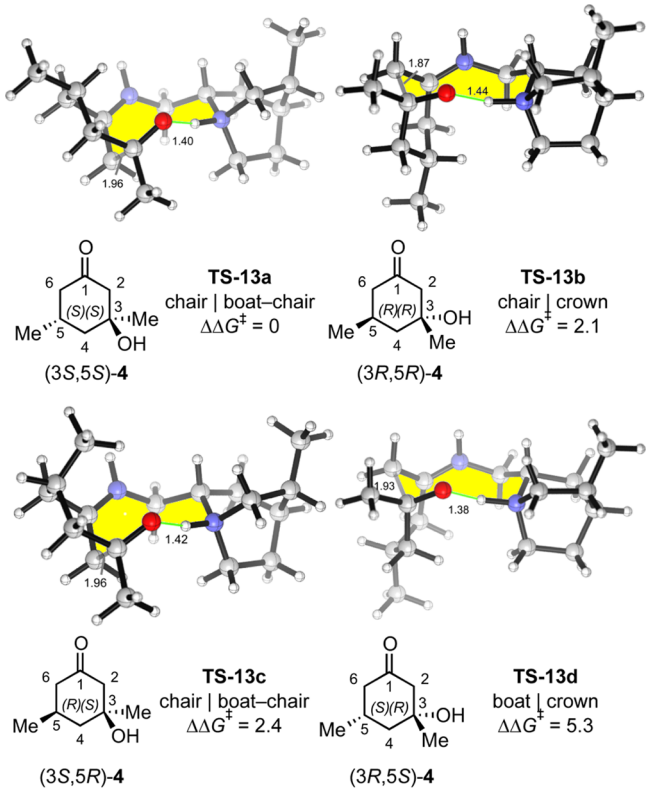

Figure 7. Lowest-energy aldol transition structures of **1** involving model catalyst **II** (B3LYP-D3(BJ)/def2-TZVPP−IEF-PCM-(toluene)//B3LYP/6-31G(d)−IEF-PCM(toluene)) for the formation of the four stereoisomers of **4**.

detail in the SI, the inclusion of dispersion with D3 and a reasonably large basis set (def2-TZVPP) provides substantial improvements in the predictions of stereoselectivity. The B3LYP-D3(BJ)/def2-TZVPP−IEF-PCM//B3LYP/6-31G(d)−IEF-PCM method is recommended for studies of this type. M06-2X/def2-TZVPP, with or without D3 corrections, is also quite good but underestimates the selectivities in some cases reported here.

CONCLUSIONS

The origins of enantiocontrol in the desymmetrizing intramolecular aldol condensations of 4-substituted heptane-2,6-diones (**1**−**3**) catalyzed by cinchona alkaloid primary amine **I** have been elucidated computationally (Scheme 5; also see the abstract graphic). The transition structures leading to the various stereoisomeric aldols incorporate hydrogen-bonded medium-sized rings with different conformations that closely resemble the well-established conformers of the cyclooctane ring. Most interestingly, the aldol transition structures show the same conformational preference as cyclooctane: both favor a boat−chair conformation. Chair | boat−chair transition structures in which both the C9 quinoline group and the diketone substituent are equatorial are the most favored. This leads to the (3*S*,5*S*) stereoisomers of the aldols, which after dehydration furnish the experimentally observed *S* enantiomers of the cyclohexenone products. The minor cyclohexenone enantiomer is predicted to originate from transition structures with the less favored chair | crown conformation in which the quinoline ring and the diketone substituent are also both equatorial. Thus, the asymmetric induction is controlled by the preferred conformation of the medium ring comprising the enamine, the acceptor carbonyl, and parts of the cinchona alkaloid scaffold. The C9 quinoline ring is predicted to be less

DOI: 10.1021/ja513096x
J. Am. Chem. Soc. 2015, 137, 2116−2127

important in stereocontrol because of its equatorial disposition on the cyclic aldol transition structures for the formation of all four aldol stereoisomers (Figure 4).

Our calculations have also shown that the origins of stereocontrol by cinchona amines can be understood with a basic knowledge of ring conformations.[34a] The intimate relationship between conformationally well-defined cyclic transition states and stereoselectivity is familiar in organic chemistry, but in the context of cinchona amine-catalyzed reactions it has rarely been exploited. The conformational preferences of medium-sized rings are the basis of numerous successful substrate-based stereocontrol strategies in organic synthesis.[79] We anticipate that an in-depth understanding of medium-ring conformations of cyclic transition states will furnish new insights into the principles of stereocontrol by cinchona alkaloid derivatives.

■ ASSOCIATED CONTENT

Supporting Information

Complete set of transition structures for aldol cyclization of **1** catalyzed by **III** (**TS-1a–p**), computational results obtained using other density functionals, computational results on enamine formation and stereoselectivity, and Cartesian coordinates and thermodynamic parameters (in hartrees) of all stationary points. This material is available free of charge via the Internet at http://pubs.acs.org.

■ AUTHOR INFORMATION

Corresponding Author

*houk@chem.ucla.edu

Notes

The authors declare no competing financial interest.

■ ACKNOWLEDGMENTS

Financial support was provided by the National Institute of General Medical Sciences, National Institutes of Health (GM36700). The computational resources from UCLA Institute for Digital Research and Education and the National Science Foundation through XSEDE resources provided by the XSEDE Science Gateways Program (TG-CHE040013N) are gratefully acknowledged.

■ REFERENCES

(1) Zhou, J.; Wakchaure, V.; Kraft, P.; List, B. *Angew. Chem., Int. Ed.* **2008**, *47*, 7656–7658.

(2) (a) Brunner, H.; Bügler, J.; Nuber, B. *Tetrahedron: Asymmetry* **1995**, *6*, 1699–1702. (b) Cassani, C.; Martín-Rapún, R.; Arceo, E.; Bravo, F.; Melchiorre, P. *Nat. Protoc.* **2013**, *8*, 325–344.

(3) Agami, C.; Sevestre, H. *J. Chem. Soc., Chem. Commun.* **1984**, 1385–1386.

(4) Clemente, F. R.; Houk, K. N. *J. Am. Chem. Soc.* **2005**, *127*, 11294–11302.

(5) List, B.; Lerner, R. A.; Barbas, C. F., III. *Org. Lett.* **1999**, *1*, 59–62.

(6) For a recent review of asymmetric organocatalytic methods to access chiral cyclohexenone skeletons, see: Yang, X.; Wang, J.; Li, P. *Org. Biomol. Chem.* **2014**, *12*, 2499–2513.

(7) (a) Zheng, B.-L.; Liu, Q.-Z.; Guo, C.-S.; Wang, X.-L.; He, L. *Org. Biomol. Chem.* **2007**, *5*, 2913–2915. (b) Perera, S.; Naganaboina, V. K.; Wang, L.; Zhang, B.; Guo, Q.; Rout, L.; Zhao, C.-G. *Adv. Synth. Catal.* **2011**, *353*, 1729–1734. (c) Guo, Q.; Zhao, J. C.-G. *Tetrahedron Lett.* **2012**, *53*, 1768–1771. (d) Corbett, M. T.; Johnson, J. S. *Angew. Chem., Int. Ed.* **2014**, *53*, 255–259.

(8) Bahmanyar, S.; Houk, K. N. *J. Am. Chem. Soc.* **2001**, *123*, 12911–12912.

(9) Clemente, F. R.; Houk, K. N. *Angew. Chem., Int. Ed.* **2004**, *43*, 5766–5768.

(10) Hoang, L.; Bahmanyar, S.; Houk, K. N.; List, B. *J. Am. Chem. Soc.* **2003**, *125*, 16–17.

(11) Bahmanyar, S.; Houk, K. N.; Martin, H. J.; List, B. *J. Am. Chem. Soc.* **2003**, *125*, 2475–2479.

(12) List, B.; Lerner, R. A.; Barbas, C. F., III. *J. Am. Chem. Soc.* **2000**, *122*, 2395–2396.

(13) The stereoisomeric transition states for the proline-catalyzed aldol additions have been revisited by Rzepa recently. See: Armstrong, A.; Boto, R.; Dingwall, P.; Contreras-García, J.; Harvey, M. J.; Mason, N. J.; Rzepa, H. S. *Chem. Sci.* **2014**, *5*, 2057–2071.

(14) (a) Albrecht, Ł.; Jiang, H.; Jørgensen, K. A. *Chem.—Eur. J.* **2014**, *20*, 358–368. (b) Nielsen, M.; Worgull, D.; Zweifel, T.; Gschwend, B.; Bertelsen, S.; Jørgensen, K. A. *Chem. Commun.* **2011**, 632–649. (c) Pihko, P. M.; Majander, I.; Erkkilä, A. *Top. Curr. Chem.* **2009**, *291*, 29–74. (d) Mukherjee, S.; Yang, J. W.; Hoffmann, S.; List, B. *Chem. Rev.* **2007**, *107*, 5471–5569. (e) Saito, S.; Yamamoto, H. *Acc. Chem. Res.* **2004**, *37*, 570–579.

(15) Seebach, D.; Goliński, J. *Helv. Chim. Acta* **1981**, *64*, 1413–1423.

(16) (a) Stegbauer, L.; Sladojevich, F.; Dixon, D. J. *Chem. Sci.* **2012**, *3*, 942–958. (b) Marcelli, T. *Wiley Interdiscip. Rev.: Comput. Mol. Sci.* **2011**, *1*, 142–152. (c) Yeboah, E. M. O.; Yeboah, S. O.; Singh, G. S. *Tetrahedron* **2011**, *67*, 1725–1762. (d) Marcelli, T.; Hiemstra, H. *Synthesis* **2010**, 1229–1279. (e) Connon, S. J. *Chem. Commun.* **2008**, 2499–2510.

(17) (a) Duan, J.; Li, P. *Catal. Sci. Technol.* **2014**, *4*, 311–320. (b) Melchiorre, P. *Angew. Chem., Int. Ed.* **2012**, *51*, 9748–9770. (c) Jiang, L.; Chen, Y.-C. *Catal. Sci. Technol.* **2011**, *1*, 354–365. (d) Bartoli, G.; Melchiorre, P. *Synlett* **2008**, 1759–1772.

(18) (a) Ingemann, S.; Hiemstra, H. Cinchonas and Cupreidines. In *Comprehensive Enantioselective Organocatalysis: Catalysts, Reactions, and Applications*; Dalko, P. I., Ed.; Wiley-VCH: Weinheim, Germany, 2013; Vol. *1*, pp 119–160. (b) Li, H.; Chen, Y.; Deng, L. Cinchona Alkaloids. In *Privileged Chiral Ligands and Catalysts*; Zhou, Q.-L., Ed.; Wiley-VCH: Weinheim, Germany, 2011; pp 361–408. (c) Song, C. E. An Overview of Cinchona Alkaloids in Chemistry. In *Cinchona Alkaloids in Synthesis and Catalysis: Ligands, Immobilization and Organocatalysis*; Song, C. E., Ed.; Wiley-VCH: Weinheim, Germany, 2009; pp 1–10.

(19) Lifchits, O.; Mahlau, M.; Reisinger, C. M.; Lee, A.; Farès, C.; Polyak, I.; Gopakumar, G.; Thiel, W.; List, B. *J. Am. Chem. Soc.* **2013**, *135*, 6677–6693.

(20) Moran, A.; Hamilton, A.; Bo, C.; Melchiorre, P. *J. Am. Chem. Soc.* **2013**, *135*, 9091–9098.

(21) (a) Bartoli, G.; Bosco, M.; Carlone, A.; Pesciaioli, F.; Sambri, L.; Melchiorre, P. *Org. Lett.* **2007**, *9*, 1403–1405. (b) Chen, W.; Du, W.; Yue, L.; Li, R.; Wu, Y.; Ding, L.-S.; Chen, Y.-C. *Org. Biomol. Chem.* **2007**, *5*, 816–821.

(22) (a) Su, Z.; Lee, H. W.; Kim, C. K. *Eur. J. Org. Chem.* **2013**, 1706–1715. (b) Oliva, C. G.; Silva, A. M. S.; Resende, D. I. S. P.; Paz, F. A. A.; Cavaleiro, J. A. S. *Eur. J. Org. Chem.* **2010**, 3449–3458.

(23) Hintermann, L.; Ackerstaff, J.; Boeck, F. *Chem.—Eur. J.* **2013**, *19*, 2311–2321.

(24) (a) Sengupta, A.; Sunoj, R. B. *J. Org. Chem.* **2012**, *77*, 10525–10536. (b) Amere, M.; Lasne, M.-C.; Rouden, J. *Org. Lett.* **2007**, *9*, 2621–2624.

(25) Zhu, J.-L.; Zhang, Y.; Liu, C.; Zheng, A.-M.; Wang, W. *J. Org. Chem.* **2012**, *77*, 9813–9825.

(26) Cucinotta, C. S.; Kosa, M.; Melchiorre, P.; Cavalli, A.; Gervasio, F. L. *Chem.—Eur. J.* **2009**, *15*, 7913–7921.

(27) (a) Yang, H.; Wong, M. W. *J. Am. Chem. Soc.* **2013**, *135*, 5808–5818. (b) Chen, Y.; Tian, S.-K.; Deng, L. *J. Am. Chem. Soc.* **2000**, *122*, 9542–9543.

(28) (a) Xue, X.-S.; Li, X.; Yu, A.; Yang, C.; Song, C.; Cheng, J.-P. *J. Am. Chem. Soc.* **2013**, *135*, 7462–7473. (b) Wu, Y.; Singh, R. P.; Deng, L. *J. Am. Chem. Soc.* **2011**, *133*, 12458–12461.

(29) Cook, T. C.; Andrus, M. B.; Ess, D. H. *Org. Lett.* **2012**, *14*, 5836–5839.

DOI: 10.1021/ja513096x
J. Am. Chem. Soc. 2015, 137, 2116–2127

(30) de Freitas Martins, E.; Pliego, J. R., Jr. *ACS Catal.* **2013**, *3*, 613−616.
(31) O'Donnell, M. J.; Bennett, W. D.; Wu, S. *J. Am. Chem. Soc.* **1989**, *111*, 2353−2355.
(32) Corey, E. J.; Xu, F.; Noe, M. C. *J. Am. Chem. Soc.* **1997**, *119*, 12414−12415.
(33) (a) Denmark, S. E.; Gould, N. D.; Wolf, L. M. *J. Org. Chem.* **2011**, *76*, 4260−4336. (b) Denmark, S. E.; Gould, N. D.; Wolf, L. M. *J. Org. Chem.* **2011**, *76*, 4337−4357.
(34) (a) Lam, Y.-h.; Houk, K. N. *J. Am. Chem. Soc.* **2014**, *136*, 9556−9559. (b) Kwiatkowski, P.; Beeson, T. D.; Conrad, J. C.; MacMillan, D. W. C. *J. Am. Chem. Soc.* **2011**, *133*, 1738−1741.
(35) (a) Scheffler, U.; Mahrwald, R. *Chem.—Eur. J.* **2013**, *19*, 14346−14396. (b) Trost, B. M.; Brindle, C. S. *Chem. Soc. Rev.* **2010**, *39*, 1600−1632. (c) *Modern Methods in Stereoselective Aldol Reactions*; Mahrwald, R., Ed.; Wiley-VCH: Weinheim, Germany, 2013. (d) *Aldol Reactions*; Mahrwald, R., Ed.; Springer: Dordrecht, The Netherlands, 2009. (e) Geary, L. M.; Hultin, P. G. *Tetrahedron: Asymmetry* **2009**, *20*, 131−173. (f) Palomo, C.; Oiarbide, M.; García, J. M. *Chem. Soc. Rev.* **2004**, *33*, 65−75. (g) Machajewski, T. D.; Wong, C.-H. *Angew. Chem., Int. Ed.* **2000**, *39*, 1352−1375.
(36) Dijkstra, G. D. H.; Kellogg, R. M.; Wynberg, H.; Svendsen, J. S.; Marko, I.; Sharpless, K. B. *J. Am. Chem. Soc.* **1989**, *111*, 8069−8076.
(37) (a) Dijkstra, G. D. H.; Kellogg, R. M.; Wynberg, H. *J. Org. Chem.* **1990**, *55*, 6121−6131. (b) Bürgi, T.; Baiker, A. *J. Am. Chem. Soc.* **1998**, *120*, 12920−12926. (c) Brunner, H.; Schmidt, P.; Prommesberger, M. *Tetrahedron: Asymmetry* **2000**, *11*, 1501−1512. (d) Maier, N. M.; Schefzick, S.; Lombardo, G. M.; Feliz, M.; Rissanen, K.; Lindner, W.; Lipkowitz, K. B. *J. Am. Chem. Soc.* **2002**, *124*, 8611−8629. (e) Urakawa, A.; Meier, D. M.; Rüegger, H.; Baiker, A. *J. Phys. Chem. A* **2008**, *112*, 7250−7255. (f) Busygin, I.; Nieminen, V.; Taskinen, A.; Sinkkonen, J.; Toukoniitty, E.; Sillanpää, R.; Murzin, D. Y.; Leino, R. *J. Org. Chem.* **2008**, *73*, 6559−6569. (g) Prakash, G. K. S.; Wang, F.; Ni, C.; Shen, J.; Haiges, R.; Yudin, A. K.; Mathew, T.; Olah, G. A. *J. Am. Chem. Soc.* **2011**, *133*, 9992−9995. (h) Tanzer, E.-M.; Schweizer, W. B.; Ebert, M.-O.; Gilmour, R. *Chem.—Eur. J.* **2012**, *18*, 2006−2013. (i) Sen, A.; Lepere, V.; Le Barbu-Debus, K.; Zehnacker, A. *ChemPhysChem* **2013**, *14*, 3559−3568. (j) Prakash, G. K. S.; Wang, F.; Rahm, M.; Zhang, Z.; Ni, C.; Shen, J.; Olah, G. A. *J. Am. Chem. Soc.* **2014**, *136*, 10418−10431.
(38) Olsen, R. A.; Borchardt, D.; Mink, L.; Agarwal, A.; Mueller, L. J.; Zaera, F. *J. Am. Chem. Soc.* **2006**, *128*, 15594−15595.
(39) Frisch, M. J.; Trucks, G. W.; Schlegel, H. B.; Scuseria, G. E.; Robb, M. A.; Cheeseman, J. R.; Scalmani, G.; Barone, V.; Mennucci, B.; Petersson, G. A.; Nakatsuji, H.; Caricato, M.; Li, X.; Hratchian, H. P.; Izmaylov, A. F.; Bloino, J.; Zheng, G.; Sonnenberg, J. L.; Hada, M.; Ehara, M.; Toyota, K.; Fukuda, R.; Hasegawa, J.; Ishida, M.; Nakajima, T.; Honda, Y.; Kitao, O.; Nakai, H.; Vreven, T.; Montgomery, J. A., Jr.; Peralta, J. E.; Ogliaro, F.; Bearpark, M.; Heyd, J. J.; Brothers, E.; Kudin, K. N.; Staroverov, V. N.; Keith, T.; Kobayashi, R.; Normand, J.; Raghavachari, K.; Rendell, A.; Burant, J. C.; Iyengar, S. S.; Tomasi, J.; Cossi, M.; Rega, N.; Millam, J. M.; Klene, M.; Knox, J. E.; Cross, J. B.; Bakken, V.; Adamo, C.; Jaramillo, J.; Gomperts, R.; Stratmann, R. E.; Yazyev, O.; Austin, A. J.; Cammi, R.; Pomelli, C.; Ochterski, J. W.; Martin, R. L.; Morokuma, K.; Zakrzewski, V. G.; Voth, G. A.; Salvador, P.; Dannenberg, J. J.; Dapprich, S.; Daniels, A. D.; Farkas, Ö.; Foresman, J. B.; Ortiz, J. V.; Cioslowski, J.; Fox, D. J. *Gaussian 09*, revision D.01; Gaussian, Inc.: Wallingford, CT, 2013.
(40) (a) Vosko, S. H.; Wilk, L.; Nusair, M. *Can. J. Phys.* **1980**, *58*, 1200−1211. (b) Lee, C.; Yang, W.; Parr, R. G. *Phys. Rev. B* **1988**, *37*, 785−789. (c) Becke, A. D. *J. Chem. Phys.* **1993**, *98*, 5648−5652. (d) Stephens, P. J.; Devlin, F. J.; Chabalowski, C. F.; Frisch, M. J. *J. Phys. Chem.* **1994**, *98*, 11623−11627.
(41) Tomasi, J.; Mennucci, B.; Cammi, R. *Chem. Rev.* **2005**, *105*, 2999−3094.
(42) Grimme, S.; Antony, J.; Ehrlich, S.; Krieg, H. *J. Chem. Phys.* **2010**, *132*, No. 154104.
(43) (a) Grimme, S.; Ehrlich, S.; Goerigk, L. *J. Comput. Chem.* **2011**, *32*, 1456−1465. (b) Johnson, E. R.; Becke, A. D. *J. Chem. Phys.* **2006**, *124*, No. 174104. (c) Johnson, E. R.; Becke, A. D. *J. Chem. Phys.* **2005**, *123*, No. 024101.
(44) Goerigk, L.; Grimme, S. *Phys. Chem. Chem. Phys.* **2011**, *13*, 6670−6688.
(45) Weigend, F.; Ahlrichs, R. *Phys. Chem. Chem. Phys.* **2005**, *7*, 3297−3305.
(46) (a) Ribeiro, R. F.; Marenich, A. V.; Cramer, C. J.; Truhlar, D. G. *J. Phys. Chem. B* **2011**, *115*, 14556−14562. (b) Zhao, Y.; Truhlar, D. G. *Phys. Chem. Chem. Phys.* **2008**, *10*, 2813−2818.
(47) Zhao, Y.; Truhlar, D. *Theor. Chem. Acc.* **2008**, *120*, 215−241.
(48) (a) Cheong, P. H.-Y.; Legault, C. Y.; Um, J. M.; Çelebi-Ölçüm, N.; Houk, K. N. *Chem. Rev.* **2011**, *111*, 5042−5137. (b) Allemann, C.; Gordillo, R.; Clemente, F. R.; Cheong, P. H.-Y.; Houk, K. N. *Acc. Chem. Res.* **2004**, *37*, 558−569.
(49) (a) Waller, M.; Grimme, S. Weak Intermolecular Interactions: A Supermolecular Approach. In *Handbook of Computational Chemistry*; Leszczynski, J., Ed.; Springer: Dordrecht, The Netherlands, 2012; pp 443−466. (b) Grimme, S. *Wiley Interdiscip. Rev.: Comput. Mol. Sci.* **2011**, *1*, 211−228.
(50) Simón, L.; Goodman, J. M. *Org. Biomol. Chem.* **2011**, *9*, 689−700.
(51) For a recent large-scale evaluation of several quantum-chemical methods in the calculation of noncovalent interactions, including a timing analysis of different density functionals, see: Li, A.; Muddana, H. S.; Gilson, M. K. *J. Chem. Theory Comput.* **2014**, *10*, 1563−1575.
(52) Krenske, E. H.; Houk, K. N. *Acc. Chem. Res.* **2013**, *46*, 979−989.
(53) (a) Wang, H.; Jain, P.; Antilla, J. C.; Houk, K. N. *J. Org. Chem.* **2013**, *78*, 1208−1215. (b) Pham, H. V.; Martin, D. B. C.; Vanderwal, C. D.; Houk, K. N. *Chem. Sci.* **2012**, *3*, 1650−1655. (c) DiRocco, D. A.; Noey, E. L.; Houk, K. N.; Rovis, T. *Angew. Chem., Int. Ed.* **2012**, *51*, 2391−2394. (d) Um, J. M.; DiRocco, D. A.; Noey, E. L.; Rovis, T.; Houk, K. N. *J. Am. Chem. Soc.* **2011**, *133*, 11249−11254. (e) Krenske, E. H.; Houk, K. N.; Harmata, M. *Org. Lett.* **2010**, *12*, 444−447.
(54) (a) Kótai, B.; Kardos, G.; Hamza, A.; Farkas, V.; Pápai, I.; Soós, T. *Chem.—Eur. J.* **2014**, *20*, 5631−5639. (b) Krenske, E. H. *Org. Biomol. Chem.* **2013**, *11*, 5226−5232. (c) Grayson, M. N.; Goodman, J. M. *J. Am. Chem. Soc.* **2013**, *135*, 6142−6148. (d) Shibata, Y.; Yamanaka, M. *J. Org. Chem.* **2013**, *78*, 3731−3736. (e) Yamanaka, M.; Hoshino, M.; Katoh, T.; Mori, K.; Akiyama, T. *Eur. J. Org. Chem.* **2012**, 4508−4514.
(55) Schwabe, T.; Huenerbein, R.; Grimme, S. *Synlett* **2010**, 1431−1441.
(56) MacroModel, version 9.9; Schrödinger, LLC: New York, 2012.
(57) Banks, J. L.; Beard, H. S.; Cao, Y.; Cho, A. E.; Damm, W.; Farid, R.; Felts, A. K.; Halgren, T. A.; Mainz, D. T.; Maple, J. R.; Murphy, R.; Philipp, D. M.; Repasky, M. P.; Zhang, L. Y.; Berne, B. J.; Friesner, R. A.; Gallicchio, E.; Levy, R. M. *J. Comput. Chem.* **2005**, *26*, 1752−1780.
(58) An excess of acid cocatalyst (2−3-fold relative to the organocatalyst) is also optimal in iminium-activated transformations catalyzed by **I**. Melchiorre recently reported a detailed mechanistic investigation of the cinchona amine-catalyzed Michael addition of indole nucleophiles to α,β-unsaturated ketones in toluene (ref 20). It was experimentally determined that the excess acid accelerates the formation of the iminium ion but that the enantioselectivity is insensitive to the amount of the cocatalyst used.
(59) Minder, B.; Mallat, T.; Skrabal, P.; Baiker, A. *Catal. Lett.* **1994**, *29*, 115−124.
(60) Cinchonine. In *The Merck Index Online*; Royal Society of Chemistry: Cambridge, U.K.; https://www.rsc.org/Merck-Index/monograph/mono1500002290 (accessed June 16, 2014).
(61) (a) Zhu, X.; Tanaka, F.; Lerner, R. A.; Barbas, C. F., III; Wilson, I. A. *J. Am. Chem. Soc.* **2009**, *131*, 18206−18207. (b) List, B. *Acc. Chem. Res.* **2004**, *37*, 548−557.
(62) See the Supporting Information for details.
(63) Wang, H.; Houk, K. N. *Chem. Sci.* **2014**, *5*, 462−470.
(64) Wiberg, K. B. *J. Org. Chem.* **2003**, *68*, 9322−9329.
(65) Rocha, W. R.; Pliego, J. R.; Resende, S. M.; Dos Santos, H. L. F.; De Oliveira, M. A.; De Almeida, W. B. *J. Comput. Chem.* **1998**, *19*, 524−534.

DOI: 10.1021/ja513096x
J. Am. Chem. Soc. 2015, 137, 2116−2127

(66) Evans, D. G.; Boeyens, J. C. A. *Acta Crystallogr., Sect. B: Struct. Sci.* **1988**, *44*, 663−671.
(67) (a) Anet, F. A. L. *Top. Curr. Chem.* **1974**, *45*, 169−220. (b) Dunitz, J. D. *Pure Appl. Chem.* **1971**, *25*, 495−508.
(68) Pakes, P. W.; Rounds, T. C.; Strauss, H. L. *J. Phys. Chem.* **1981**, *85*, 2469−2475.
(69) (a) Anet, F. A. L.; Basus, V. J. *J. Am. Chem. Soc.* **1973**, *95*, 4424−4426. (b) Meiboom, S.; Hewitt, R. C.; Luz, Z. *J. Chem. Phys.* **1977**, *66*, 4041−4051. (c) Dorofeeva, O. V.; Mastryukov, V. S.; Allinger, N. L.; Almenningen, A. *J. Phys. Chem.* **1985**, *89*, 252−257.
(70) At the B3LYP-D3(BJ)/def2-TZVPP−IEF-PCM(toluene)//B3LYP/6-31G(d)−IEF-PCM(toluene) level of theory, the crown conformation is higher in free energy than the boat−chair conformation by 1.3 kcal/mol, while the boat−boat conformation is less stable by 4.2 kcal/mol.
(71) Zimmerman, H. E.; Traxler, M. D. *J. Am. Chem. Soc.* **1957**, *79*, 1920−1923.
(72) In most cases, the vinyl group on the quinuclidine ring has little influence over the sense of asymmetric induction in reactions organocatalyzed by cinchona alkaloid derivatives. For a rare example in which the identity of this ring substituent dramatically affects the product outcome in an organocatalyzed reaction, see: Qian, H.; Yu, X.; Zhang, J.; Sun, J. *J. Am. Chem. Soc.* **2013**, *135*, 18020−18023.
(73) Model catalyst **II** is the same as the known primary amine derived from substitution of the hydroxyl group of quincorine, save for the replacement of the methyl group on the quinuclidine moiety of **II** by a vinyl group. For the first preparation of the primary amines derived from quincorine and the pseudoenantiomeric quincoridine, see: (a) Schrake, O.; Franz, M. H.; Wartchow, R.; Hoffmann, H. M. R. *Tetrahedron* **2000**, *56*, 4453−4465. For a review, see: (b) Hoffmann, H. M. R.; Frackenpohl, J. *Eur. J. Org. Chem.* **2004**, 4293−4312.
(74) Quincorine- and quincoridine-derived amines have been reported as organocatalysts less frequently than amines based on quinine and cinchonidine or their pseudoenantiomers. For examples, see: (a) Kündig, E. P.; Garcia, A. E.; Lomberget, T.; Garcia, P. P.; Romanens, P. *Chem. Commun.* **2008**, 3519−3521. In some cases, the use of cinchona amines bearing the quinoline group is superior. See: (b) Lee, A.; Michrowska, A.; Sulzer-Mosse, S.; List, B. *Angew. Chem., Int. Ed.* **2011**, *50*, 1707−1710. (c) Armstrong, A.; Pullin, R. D. C.; Jenner, C. R.; Foo, K.; White, A. J. P.; Scutt, J. N. *Tetrahedron: Asymmetry* **2014**, *25*, 74−86.
(75) Work is in progress to verify this prediction experimentally. Full discussion of these experimental and computational results will be disclosed in due course.
(76) (a) Cohen, A. J.; Mori-Sánchez, P.; Yang, W. *Chem. Rev.* **2012**, *112*, 289−320. (b) Hobza, P. *Acc. Chem. Res.* **2012**, *45*, 663−672. (c) Burns, L. A.; Mayagoitia, A. V.; Sumpter, B. G.; Sherrill, C. D. *J. Chem. Phys.* **2011**, *134*, No. 084107. (d) Johnson, E. R.; Mackie, I. D.; DiLabio, G. A. *J. Phys. Org. Chem.* **2009**, *22*, 1127−1135. (e) Foster, M. E.; Sohlberg, K. *Phys. Chem. Chem. Phys.* **2010**, *12*, 307−322. (f) Schwabe, T.; Grimme, S. *Acc. Chem. Res.* **2008**, *41*, 569−579. (g) Johnston, R. C.; Cheong, P. H.-Y. *Org. Biomol. Chem.* **2013**, *11*, 5057−5064.
(77) Kruse, H.; Goerigk, L.; Grimme, S. *J. Org. Chem.* **2012**, *77*, 10824−10834.
(78) The importance of dispersion effects in stereocontrol in organocatalytic reactions has also been described by Uyeda and Jacobsen, who found that the stereoselectivities computed using the dispersion-inclusive M05-2X functional for a guanidinium-catalyzed enantioselective Claisen rearrangement correlate better with experiment than those computed using B3LYP. See: Uyeda, C.; Jacobsen, E. N. *J. Am. Chem. Soc.* **2011**, *133*, 5062−5075.
(79) (a) Carreira, E. M.; Kvaerno, L. Macrocyclic Stereocontrol. In *Classics in Stereoselective Synthesis*; Wiley-VCH: Weinheim, Germany, 2009; pp 1−17. (b) Still, W. C.; Galynker, I. *Tetrahedron* **1981**, *37*, 3981−3996. (c) Still, W. C.; MacPherson, L. J.; Harada, T.; Callahan, J. F.; Rheingold, A. L. *Tetrahedron* **1984**, *40*, 2275−2281.

DOI: 10.1021/ja513096x
J. Am. Chem. Soc. 2015, 137, 2116−2127